BIOPHYSICS

MyoD-family inhibitor proteins act as auxiliary subunits of Piezo channels

Zijing Zhou[1,2]†, Xiaonuo Ma[3,4]†, Yiechang Lin[5], Delfine Cheng[1,2], Navid Bavi[6], Genevieve A. Secker[7], Jinyuan Vero Li[1,2], Vaibhao Janbandhu[1,2], Drew L. Sutton[7,8], Hamish S. Scott[7,8,9], Mingxi Yao[10], Richard P. Harvey[1,2,11], Natasha L. Harvey[7,8], Ben Corry[5], Yixiao Zhang[3,4]*, Charles D. Cox[1,12]*

Piezo channels are critical cellular sensors of mechanical forces. Despite their large size, ubiquitous expression, and irreplaceable roles in an ever-growing list of physiological processes, few Piezo channel–binding proteins have emerged. In this work, we found that MyoD (myoblast determination)–family inhibitor proteins (MDFIC and MDFI) are PIEZO1/2 interacting partners. These transcriptional regulators bind to PIEZO1/2 channels, regulating channel inactivation. Using single-particle cryogenic electron microscopy, we mapped the interaction site in MDFIC to a lipidated, C-terminal helix that inserts laterally into the PIEZO1 pore module. These Piezo-interacting proteins fit all the criteria for auxiliary subunits, contribute to explaining the vastly different gating kinetics of endogenous Piezo channels observed in many cell types, and elucidate mechanisms potentially involved in human lymphatic vascular disease.

To decode mechanical cues, cells are endowed with a palette of molecular force sensors. Among these sensors, Piezo ion channels (*1*) have emerged as critical force sensors that participate in determining how cells sense their physical environment.

Piezo channels assemble as trimers that possess all the structural requirements for mechanosensitivity (*2*, *3*). However, native PIEZO1 channels can display nonuniform subcellular localization (*4*–*7*) and exhibit different gating kinetics—principally, slower inactivation (*1*, *8*–*13*)—in many cell types when compared with heterologous expression systems. These observations could be explained by differences in lipid composition (*14*, *15*), curvature-dependent sorting (*5*, *7*), or protein-protein interactions. Many ion channels interact with auxiliary subunits (*16*, *17*) to modify their cellular location and gating properties. Ion-channel auxiliary subunits are commonly defined by four criteria: (i) they are non–pore-forming subunits, (ii) they have a direct and stable interaction with the pore-forming subunit, (iii) they modulate channel properties in heterologous systems, and (iv) they regulate endogenous channel activity in native cells (*17*). Despite substantial effort, to our knowledge, no Piezo channel–binding partners or auxiliary subunits have emerged that fit these criteria.

Identification of Piezo channel–binding proteins

To identify binding partners for Piezo channels we used two complementary affinity-capture mass spectrometry (AC-MS) strategies in conjunction with two CRISPR-Cas9–edited, PIEZO1-expressing, human dermal fibroblast (hDF) lines (Fig. 1, A to F, and fig. S1). The reason we chose fibroblasts lies in the previously reported slower inactivation kinetics of PIEZO1 in this cell type (*10*, *12*, *13*). Our pipeline consisted of three comparator groups: (i) hDF with PIEZO1 ablated with CRISPR/cas9 (that were compared with wild-type cells in which PIEZO1 was enriched through a conventional anti-PIEZO1 antibody strategy), (ii) hDF with a HaloTag added into the endogenous PIEZO1 loci (P1-Halo) where PIEZO1 was enriched with HaloTrap resin, and (iii) primary human cardiac fibroblasts (hCF) in which PIEZO1 was enriched through a conventional anti-PIEZO1 antibody strategy. We then stringently analyzed the resulting MS data to identify PIEZO1-interacting proteins present in all three groups that were not present in any of their respective negative controls. Using these criteria, we only identified two proteins, the first of which was PIEZO1 (Fig. 1E). This provided strong validation for both affinity-capture strategies. The second protein identified was the sparsely studied transcriptional regulator MyoD (myoblast determination) family–inhibitor domain-containing protein (MDFIC) (*18*, *19*). MS provided 39 ± 14% coverage of MDFIC protein averaged over the three groups (Fig. 1F).

Using RNA expression data, we identified many cell types in addition to fibroblasts that coexpress Piezo channels and the MyoD-family inhibitor proteins, MDFIC or MDFI (fig. S2, A and B) (*20*). We then validated the protein-protein interaction by expressing N-terminally hemagglutinin (HA)–tagged MDFIC together with PIEZO1 in human embryonic kidney 293 cells with SV40 large-T antigen (HEK293T). Using a coimmunoprecipitation (co-IP) assay, we could reciprocally capture PIEZO1 with MDFIC and found that the complex was present under mechanical (shear stress) or chemical [10 μM Yoda-1 (*21*)] activation of PIEZO1 (fig. S2C), which indicated the stability of the interaction. We also confirmed that PIEZO1 interacted with the closely related MDFI (fig. S2D) (*22*). PIEZO2 has high sequence similarity with PIEZO1, so we next tested whether MDFIC selectively interacted with PIEZO1/2 channels using native gels. We identified MDFIC at the size of the respective PIEZO1/2 trimers but not in oligomeric complexes of other structurally unrelated channels such as TRPM4 (tetramer) or TREK-1 (dimer) (fig. S2E). In doing so, we found that PIEZO1 enhanced the protein amounts of both MDFIC and MDFI by greater than three- to fourfold (fig. S2, C to E). To determine the specificity of this effect, we coexpressed MDFIC with PIEZO1 and PIEZO2 and compared the amount of MDFIC when expressed alongside other unrelated ion channels. Coexpression of MDFIC with green fluorescent protein (GFP), TRPM4, TRPV4, or TREK-1 did not enhance the amount of MDFIC (fig. S3, A and B). To understand the mechanism, we used a cycloheximide chase assay to observe the degradation time course of MDFIC. In cells treated for 4 to 8 hours with the protein synthesis inhibitor cycloheximide, we observed using Western blotting that the protein amount of MDFIC fell much more rapidly in the absence of PIEZO1 (fig. S3, C and D). This suggests that interacting with PIEZO1 decreased MDFIC turnover.

MDFIC binds the PIEZO1 pore module

To provide molecular details of the interaction, we coexpressed mouse PIEZO1 (mPIEZO1) with N-terminally FLAG-tagged mouse MDFIC and purified the complex using FLAG resin. Using single-particle cryogenic electron microscopy (cryo-EM), we determined the structure of the PIEZO1-MDFIC complex at an overall resolution of 3.66 Å (Fig. 2, A and B, and fig. S4). We resolved the C-terminal 21 amino acids of MDFIC (Fig. 2, A to D), whereas the N-terminal portion displayed little or no density, presumably owing to local dynamics. The resolved region of MDFIC (residues 225 to 246) consists of an amphipathic helix that sits parallel to the membrane at the membrane interface (Fig. 2C). This helix inserts laterally into the PIEZO1

[1]Victor Chang Cardiac Research Institute, Sydney, NSW 2010, Australia. [2]School of Clinical Medicine, Faculty of Medicine and Health, University of New South Wales, Sydney, NSW 2052, Australia. [3]Interdisciplinary Research Center on Biology and Chemistry, Shanghai Institute of Organic Chemistry, Chinese Academy of Sciences, Shanghai 200032, China. [4]State Key Laboratory of Chemical Biology, Shanghai Institute of Organic Chemistry, Chinese Academy of Sciences, Shanghai 200032, China. [5]Research School of Biology, Australian National University, Acton, ACT 2601, Australia. [6]Department of Biochemistry and Molecular Biophysics, University of Chicago, Chicago, IL 60637, USA. [7]Centre for Cancer Biology, University of South Australia and SA Pathology, Adelaide, SA 5001, Australia. [8]Adelaide Medical School, University of Adelaide, Adelaide, SA 5005 Australia. [9]Department of Genetics and Molecular Pathology, SA Pathology, Adelaide, SA 5000, Australia. [10]Department of Biomedical Engineering, Southern University of Science and Technology, Shenzhen 518055, China. [11]School of Biotechnology and Biomolecular Science, University of New South Wales Sydney, Kensington, NSW 2052, Australia. [12]School of Biomedical Sciences, Faculty of Medicine and Health, University of New South Wales Sydney, Kensington, NSW 2052, Australia.
*Corresponding authors. Email: c.cox@victorchang.edu.au (C.D.C.); yzhang@mail.sioc.ac.cn (Y.Z.).
†These authors contributed equally to this work.

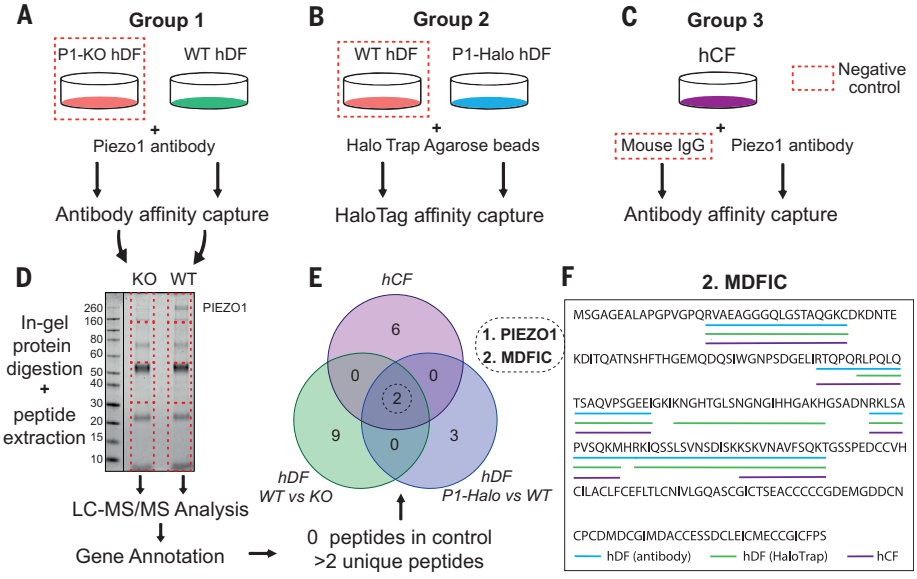

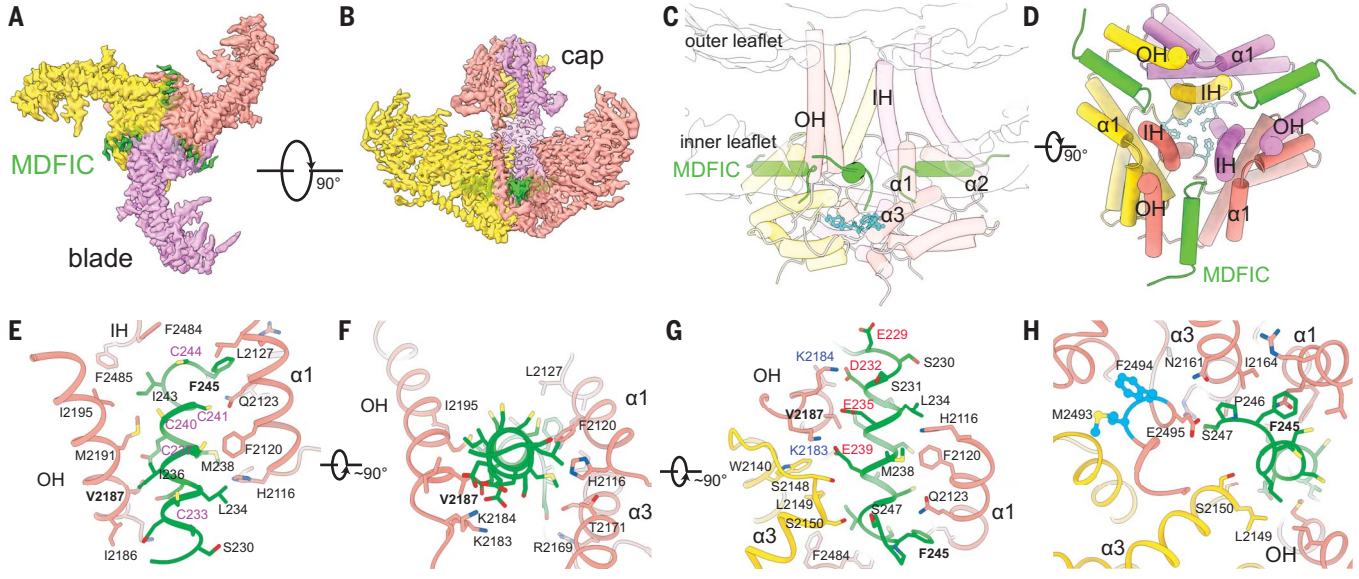

Fig. 1. AC-MS identifies a newly characterized family of Piezo-channel binding partners. Groups for AC-MS consisted of: (**A**) WT and PIEZO1-edited (knockout, KO) human dermal fibroblasts (hDF; n = 2), (**B**) WT and PIEZO1-HaloTag (P1-Halo) hDF (n = 2), and (**C**) primary human cardiac fibroblasts (hCF; n = 2). (**D**) Affinity-captured protein lysates were run on SDS–polyacrylamide gel electrophoresis (SDS-PAGE) gels and sectioned into quadrants (red dashed lines). Each quadrant was subjected to in-gel protein digestion, peptide extraction and liquid chromatography (LC), and MS, in that order. (**E**) Venn diagram illustrating proteins identified in each experimental group that had ≥2 distinct peptides that were absent from negative control replicates. (**F**) Two proteins were identified in all positive control replicates: PIEZO1 and MDFIC. Alignment of distinct MDFIC peptides identified with MS.

Fig. 2. Structural elucidation of the PIEZO1-MDFIC complex. (**A** and **B**) Cryo-EM density maps of the mouse PIEZO1-MDFIC complex at 3.66-Å nominal resolution viewed from the top (A) and side (B), with the resolved MDFIC region colored green. (**C**) The distal C-terminal of MDFIC resides parallel to the bilayer between the anchor domain (α1 to α3) and the outer helix (OH). The cytoplasmic constriction residues Met2493 and Phe2494 are shown in cyan. (**D**) The C-terminal region of MDFIC penetrates deep into the pore module of PIEZO1, approaching the inner helix (IH). (**E** to **H**) The interactions between PIEZO1 and MDFIC from the (E) membrane-facing view, (F) lateral view, and (G and H) cytoplasmic-facing view. Variants linked to lymphatic malformations (mPIEZO1 V2187 and mMDFIC F245) are labeled in bold.

pore module, nestling between the anchor domain and the outer helix of PIEZO1 (Fig. 2, C and D), making contacts with His^{2116}, Phe^{2120}, and Gln^{2123} from the α1 helix of the anchor domain; Val^{2187}, Met^{2191}, and Ile^{2195} from the outer helix; and Phe^{2484} and Phe^{2485} at the base of the inner helix that lines the PIEZO1 pore (Fig. 2E). The amphipathic helix of MDFIC consists of a sequence of five cysteines that point toward the bilayer interior (Fig. 2, E and F) and a sequence of four negatively charged residues that point toward the solvent, forming salt bridges with multiple lysine residues (Fig. 2, F and G). The MDFIC C terminus penetrates far enough to come close to the cytoplasmic constriction formed by Met^{2493} and Phe^{2494} (Fig. 2H) and residues critical for voltage-dependent inactivation, Lys^{2479} and Arg^{2482} (*23*, *24*). Despite its central location, MDFIC binding did not influence the closed structure of the PIEZO1 pore module (fig. S4I).

Because both PIEZO1 and MDFIC are essential for lymphatic development in mice and humans (*19*, *25*, *26*), we investigated using the ClinVar database whether any disease-causing mutations were located within this binding interface. We found mutations in both PIEZO1 (human V2171f; Fig. 2, E and G) and MDFIC (human F244L; Fig. 2, E and H) associated with human lymphatic disease.

MDFIC and MDFI regulate Piezo gating

Given the location of MDFIC binding, we next tested whether human MDFIC and MDFI-modified human PIEZO1 (hPIEZO1) gating in HEK293T cells. MDFIC and MDFI expressed

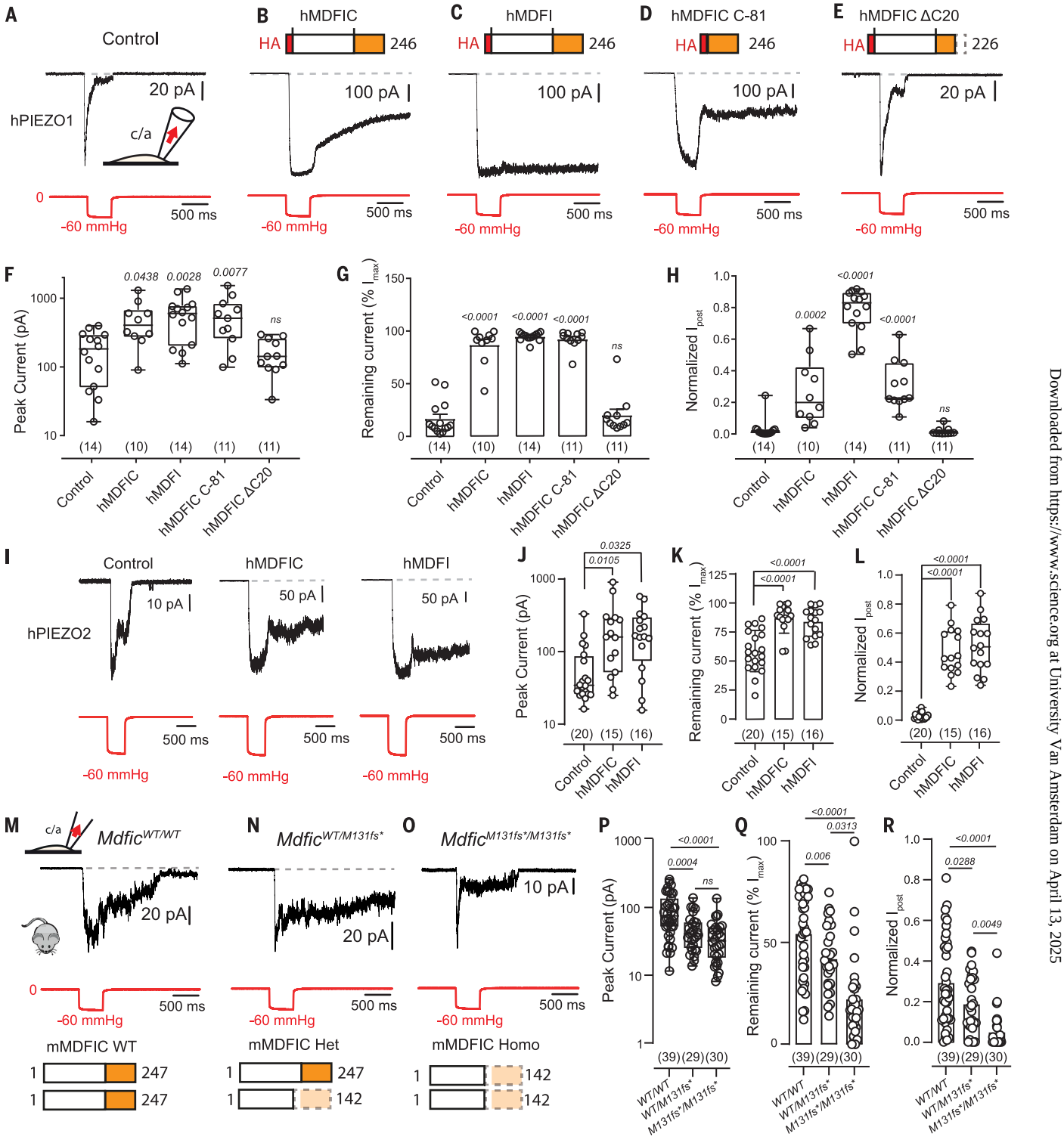

Fig. 3. MyoD-family inhibitor proteins regulate PIEZO1 and PIEZO2 channel gating. (**A** to **E**) Representative cell-attached patch-clamp recordings from hPIEZO1 (A) control and hPIEZO1 in the presence of (B) hMDFIC, (C) hMDFI, (D) the conserved C terminus of MDFIC (hMDFIC C-81), and (E) with MDFIC lacking its C-terminal 20 amino acids (hMDFIC ΔC20) all at a holding potential of −65 mV. (**F** to **H**) Quantification of (F) peak currents per patch, (G) percent current remaining, and (H) normalized current 1 s after pressure release (normalized I_{post}) for replicates of cell-attached recordings shown in (A) to (E). (**I** to **L**) Representative cell-attached recordings from (I) hPIEZO2 control and hPIEZO2 in the presence of hMDFIC and hMDFI, and [(J) to (L)] quantification of replicates. (**M** to **O**) Representative cell-attached patch-clamp recordings from mouse cardiac fibroblasts isolated at E16.5 from (M) WT, (N) heterozygous, and (O) homozygous Mdfic^{M131fs*} mice. (**P** to **R**) Quantification of (P) peak current per patch, (Q) percent current remaining, and (R) normalized I_{post} for replicates of cell-attached recordings shown in [(M) to (O)] All data are displayed as mean ± SEM or as maximum-to-minimum box-and-whiskers plot. *P* values are noted above the plots and were determined with one-way analysis of variant (ANOVA) and either Dunnett's or Tukey's multiple comparison test. ns, not significant.

alone did not generate stretch-activated currents (fig. S5, A to D). Compared with hPIEZO1 alone, coexpression with MDFIC resulted in a mild right shift in the pressure response curve [from 14.5 ± 3.2 mmHg (n = 9 cells) to 23.9 ± 3.9 mmHg (n = 6)] (fig. S5, E to G), a marked increase in the peak stretch-evoked currents, a substantial slowing of channel inactivation, and continued channel gating even after the pressure was released (Fig. 3, A to H, and fig. S5). We quantified the latter of these effects using the current that remained 1 s after application of stretch (I_{post}). Neither MDFIC nor MDFI influenced mRNA TMEM150c, demonstrating that these inactivation effects were independent of TMEM150c (fig. S5N) (*27*). MDFIC did not influence PIEZO1 protein amounts in either HEK293T or LNCaP cells transfected with MDFIC (fig. S6, A to D) but did increase PIEZO1 single-channel conductance from 26 ± 3pS (n = 4) to 48 ± 8 pS (n = 4) (fig. S6, E to G). Thus, the increase in stretch-activated currents in the presence of MDFIC is likely driven by changes in conductance and its strong

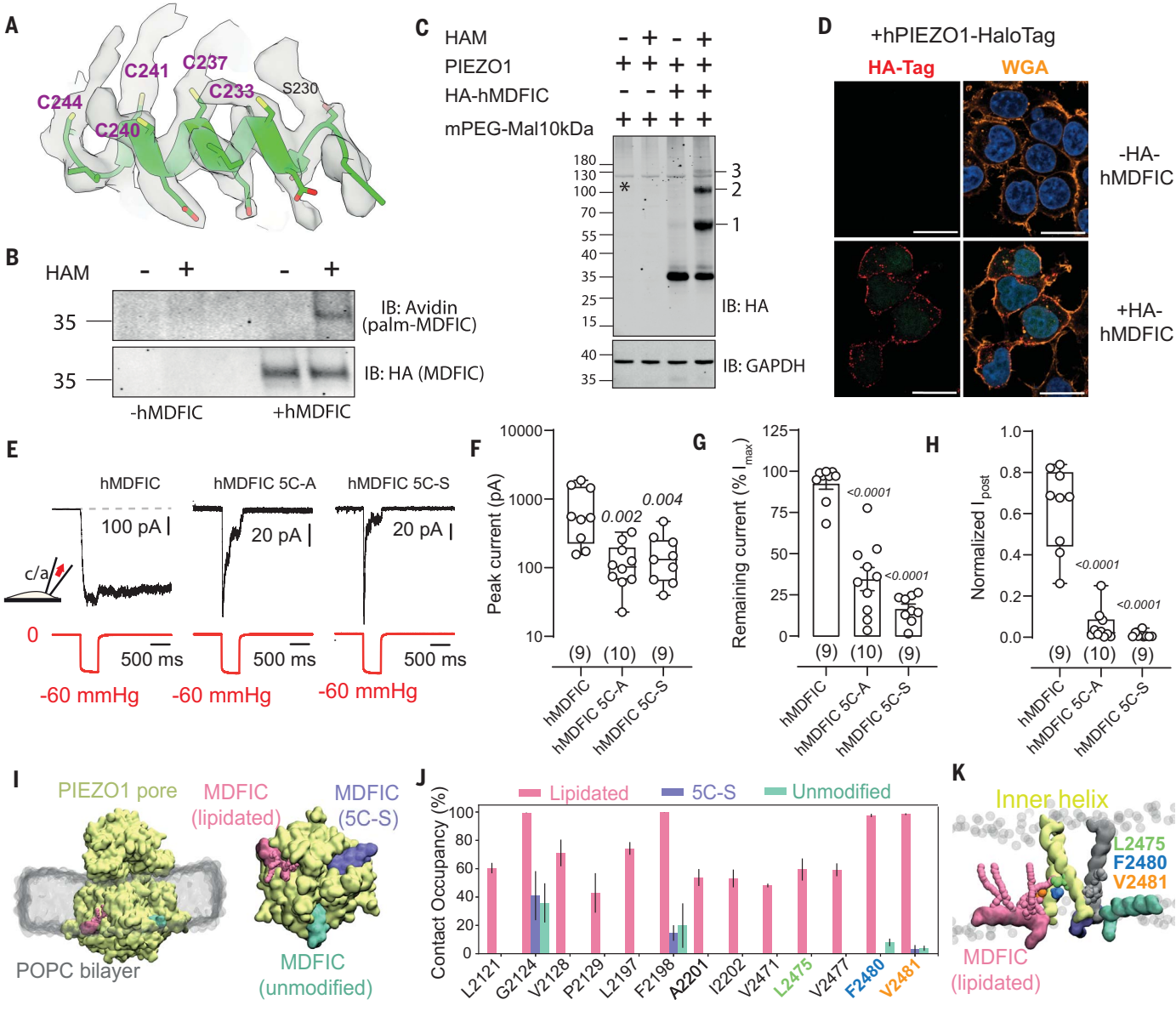

Fig. 4. C-terminal lipidation of MDFIC underlies regulation of PIEZO1 channel gating. (**A**) Cryo-EM density map showing extension of density on cysteine residues within the C terminus of MDFIC. (**B**) Representative immunoblot (IB) with Avidin (top) or anti-HA (bottom) from acyl biotin exchange showing lysate ± hydroxylamine (HAM). Blots show a band at the correct size for HA-tagged MDFIC, but the biotinylated MDFIC can only be seen in the HAM-treated group, which indicates palmitoylated-MDFIC (palm-MDFIC). (**C**) Mass-tagging of MDFIC with methoxy-polyethylene glycol (mPEGylated) maleimide reveals at least three palmitoylation sites labeled 1 to 3 (* represents a nonspecific band in all groups). (**D**) Membrane-localized HA-tagged MDFIC in PIEZO1-HaloTag expressing HEK293T cells and the wheat germ agglutinin (WGA)–delineated membrane. (**E**) Representative cell-attached recordings of hPIEZO1 in the presence of WT MDFIC and mutation of the five C-terminal cysteine residues to either alanine (5C-A) or serine (5C-S), which abolishes the regulatory effects of MDFIC. (**F** to **H**) Quantification of (F) peak currents per patch, (G) percent current remaining, and (H) normalized I_{post} for replicate recordings shown in (E). (**I**) All-atom molecular dynamic simulations of the mPIEZO1 pore module in complex with unmodified (green), 5C-S mutant (purple), and lipidated MDFIC (pink) C-termini. (**J** and **K**) Contact occupancy for MDFIC monomers with PIEZO1 residues from replicate simulations and a snapshot of the location of three inner helix residues important for inactivation that interact with lipidated MDFIC for prolonged periods. P values are noted above the plots and were determined with one-way ANOVA and Dunnett's multiple comparison test. ns, not significant.

effect on inactivation. The slow "closure" after pressure release—identified in single-channel recordings (fig. S6, H to J) and from macrocurrents—was more pronounced at hyperpolarizing voltages (fig. S7, A and B), which suggests an effect on the structural transition–governing voltage-dependent inactivation (*23*, *24*). Consistent with this, the channel could be rapidly closed by flipping the voltage to depolarizing potentials (fig. S7, C and D). We identified slower inactivation in both cell-attached and whole-cell modes (fig. S8). Additionally, MDFIC expression did not influence the function of mechanosensitive TREK-1 channels, ruling out nonspecific effects (fig. S9).

The C termini of MDFIC and MDFI are highly homologous, whereas the N termini bear little resemblance and have no known function (fig. S10A); therefore, we asked whether the MyoD-inhibitor domain of MDFIC (residues 165 to 246, which we name C-81) expressed alone could modify PIEZO1 function. Despite being unstable, this domain reduced channel inactivation (Fig. 3, D and G, and fig. S10B). Moreover, the amount of C-81 protein was dramatically increased when coexpressed with PIEZO1 (fig. S10, C and D). Conversely, truncation of the C-terminal 20 residues (ΔC20) prevented MDFIC from regulating PIEZO1 gating (Fig. 3, E to G). This truncation reduced the interaction with PIEZO1, and MDFIC ΔC20 protein amounts were only marginally affected by PIEZO1 (fig. S10, D and E). Thus, functional regulation of the PIEZO1-MDFIC complex depends on the conserved C terminus of MDFIC.

Given the homology of PIEZO1 and PIEZO2 in the MDFIC-binding region, we additionally showed that the same regulation occurs for both hPIEZO2 and mouse Piezo orthologs (Fig. 3, I to L, and fig. S11). Moreover, the expression of MDFIC and MDFI correlated with the native inactivating phenotype of PIEZO1 in multiple human and mouse cell lines (fig. S12). This included HEK293T, in which fast PIEZO1 inactivation was seen, and prostate cancer cell lines (LNCaP and DU145), in which differential stretch-activated kinetics were previously reported (*9*). HEK293T and LNCaP have almost undetectable amounts of MDFIC and MDFI and display fast inactivation, whereas DU145 has notable amounts of MDFI at the mRNA level and inactivates slowly (fig. S12, A to F). Overexpression of MDFIC in LNCaP cells markedly slowed inactivation of native PIEZO1 channels (fig. S12, B to F). In mouse embryonic fibroblasts and C2C12 myoblasts, we detected MDFIC, and both cell types displayed slow PIEZO1 inactivation indicated by larger current remaining at the end of pressure pulses (fig. S12, G to I). By contrast, in Neuro2A (N2A) cells, PIEZO1 channels exhibited rapid inactivation with undetectable expression of MDFIC and MDFI.

We next asked whether genetic loss of MDFIC could modify the kinetics of native PIEZO1 currents. To investigate this, we used a mouse model of a complex lymphatic anomaly known as central conducting lymphatic anomaly, bearing a truncated variant of MDFIC that lacked the complete conserved C-terminal but retained the N-terminal region (*19*). Our assessment of PIEZO1 activity in embryonic cardiac fibroblasts isolated from embryonic day 16.5 (E16.5) wild-type (WT/WT), heterozygous (WT/M131fs*), and homozygous mice (M131fs*/M131fs*) revealed that fibroblasts harboring C-terminally truncated MDFIC had smaller PIEZO1 currents that inactivated more rapidly (Fig. 3, M to R). This effect on inactivation was phenocopied by silencing MDFIC in fibroblasts with small interfering RNA (siRNA) (fig. S13, D to J).

PIEZO1 regulation requires MDFIC lipidation

Cryo-EM maps of MDFIC revealed extra densities on Cys^{233}, Cys^{237}, Cys^{240}, Cys^{241}, and Cys^{244} (Fig. 4A). Given that this helix is situated at the membrane interface and contains motifs for cysteine lipidation (*28*), we hypothesized that these extra densities resulted from lipidation, which is the covalent addition of acyl chains to amino acids (*29*). A second cryo-EM complex of the MDFIC mutant Cys240Ala (3.68 Å) specifically lacked the extra density at Cys^{240}, which is consistent with posttranslational modification (fig. S14). Acyl biotin exchange confirmed that MDFIC was palmitoylated (Fig. 4B). Mass tagging with polyethylene gycol–modified (PEGylated) maleimide (increases mass per palmitoylated site) showed that there were at least three sites for lipidation on MDFIC (Fig. 4C), that two were in the distal C terminus (fig. S15), and that like most lipidated proteins, MDFIC associated with the plasma membrane (Fig. 4D).

To check whether MDFIC lipidation is functionally relevant, we mutated all five C-terminal cysteines to alanine or serine. MDFIC with $Cys^{233/237/240/241/244}$Ala (5C-A) or $Cys^{233/237/240/241/244}$Ser (5C-S) bound to PIEZO1, but neither mutant influenced PIEZO1 activity, which suggests that the lipidation of the MDFIC C terminus is critical for PIEZO1 regulation (Fig. 4, E to H, and fig. S15C).

To probe the role of lipidation, we used all-atom molecular-dynamics simulations of the PIEZO1 pore module (residues 1956 to 2547) in complex with the MDFIC C terminus (Fig. 4, I to K, and fig. S16). Simulations consisted of three MDFIC monomers: one unmodified, one lipidated at all five cysteine residues in the helix, and one where each cysteine was mutated to serine (5C-S mutants) (Fig. 4I). All variations of the MDFIC C terminus remained stably bound (fig. S16, A and B). An overlay of a snapshot from simulations shows that the acyl chains coincide with the additional MDFIC cryo-EM densities (fig. S16C). We compared all interactions that occurred in either unmodified or lipidated MDFIC monomers with those in the 5C-S mutant, which we know binds to but does not modulate PIEZO1 function (Fig. 4J and fig. S16). Interactions between the unmodified and 5C-S MDFIC were indistinguishable, which supports the critical role of MDFIC lipidation in modulating PIEZO1 function. By contrast, the lipidated MDFIC had multiple distinct interactions with inner-helix residues (Fig. 4, J and K, and fig. S16, D and E). Some of these residues within the inner helix are critical for inactivation, including Leu2475 (*30*), making this the likely pathway for functional modification. Given that MDFIC would need to stay bound throughout the PIEZO1 conformational cycle, we also examined whether MDFIC could bind to the flattened state of PIEZO1 (*31*). When MDFIC was aligned to the same pocket, simulations showed that it interacted with the inner helix and remained stably bound (fig. S16, F to H).

Discussion

Using AC-MS, we have identified a family of Piezo-channel binding partners—the MyoD-family inhibitor proteins, MDFI and MDFIC—that fit all the criteria for Piezo-channel auxiliary subunits. Although our study does not resolve full-length MDFIC or its native membrane topology, it does reveal that MDFIC binds to the PIEZO1 pore module through its conserved C terminus, which regulates channel inactivation. The regulation of Piezo-channel inactivation critically involves palmitoylation of the distal C-terminal of MDFIC. Because palmitoylation is a reversible lipid addition (*29*), this adds the potential for dynamic spatiotemporal regulation of Piezo inactivation by MDFIC. Although we identified few other Piezo-channel binding-partner candidates with our "fibroblast-centric" screen, we speculate that the binding region of MDFIC could form a conserved binding site for alternate membrane-associated Piezo regulators or auxiliary subunits. In support of this hypothesis, the PIEZO1 lysine residues that form salt bridges with MDFIC have been proposed to interact with other proteins (*32*). Despite PIEZO1 channels being able to function as independent mechanosensors in simplified systems (*2*), ample evidence suggests that Piezos, particularly PIEZO2, may receive force through molecular tethers (*33*). Given the location of binding, it seems unlikely that MDFIC could act as a tethering molecule.

It remains to be seen how ubiquitous this regulatory mechanism is; MDFIC and MDFI are absent from many cell types with rapidly inactivating PIEZO1 channels, including LNCaP (*9*) and N2A (*1*), but are expressed in others, including fibroblasts (*10*, *12*, *13*) and endothelial cells that exhibit slower PIEZO1 inactivation (*8*, *11*, *14*). We isolated cardiac fibroblasts from mice that harbored a truncated MDFIC lacking the C terminus (*19*), in which PIEZO1 exhibited faster inactivation than in wild-type

fibroblasts. Thus, MDFIC- or MDFI-mediated regulation of Piezo channels could be widely used. Despite our study not defining a PIEZO1-MDFIC complex in lymphatic endothelial cells, the similar lymphatic phenotypes associated with loss of function of MDFIC (*19*) and PIEZO1 (*25*, *26*) means that this interaction may unearth molecular aspects underlying lymphatic vascular disease. Furthermore, both MDFIC and MDFI bind to transcription factors (*19*, *34*) [including GATA2, a master regulator of lymphatic valve development (*35*)]. Whether PIEZO1/2 channels influence this aspect of their function is unknown but may lay the foundation for the unveiling of a direct mechanosignaling pathway by means of Piezos to transcription through GATA2 or other transcription factors.

Thus, our structural and functional data not only reveal a family of Piezo-channel auxiliary subunits but may also reveal a conserved binding site for other membrane-associated proteins that modulate Piezo-channel function and, in doing so, the basis for an alternate Piezo-dependent mechanosignaling pathway.

REFERENCES AND NOTES

1. B. Coste *et al*., *Science* **330**, 55–60 (2010).
2. R. Syeda *et al*., *Cell Rep.* **17**, 1739–1746 (2016).
3. C. D. Cox *et al*., *Nat. Commun.* **7**, 10366 (2016).
4. M. Yao *et al*., *Sci. Adv.* **8**, eabo1461 (2022).
5. G. Vaisey, P. Banerjee, A. J. North, C. A. Haselwandter, R. MacKinnon, *eLife* **11**, e82621 (2022).
6. J. R. Holt *et al*., *eLife* **10**, e65415 (2021).
7. S. Yang *et al*., *Nat. Commun.* **13**, 7467 (2022).
8. S. Wang *et al*., *Nat. Commun.* **11**, 2303 (2020).
9. R. Maroto, A. Kurosky, O. P. Hamill, *Channels (Austin)* **6**, 290–307 (2012).
10. N. M. Blythe *et al*., *J. Biol. Chem.* **294**, 17395–17408 (2019).
11. J. I. Del Mármol, K. K. Touhara, G. Croft, R. MacKinnon, *eLife* **7**, e33149 (2018).
12. E. Glogowska *et al*., *Cell Rep.* **37**, 110070 (2021).
13. D. Jakob *et al*., *J. Mol. Cell. Cardiol.* **158**, 49–62 (2021).
14. J. Shi *et al*., *Cell Rep.* **33**, 108225 (2020).
15. L. O. Romero *et al*., *Nat. Commun.* **10**, 1200 (2019).
16. A. C. Dolphin, *J. Physiol.* **594**, 5369–5390 (2016).
17. D. Yan, S. Tomita, *J. Physiol.* **590**, 21–31 (2012).
18. S. Thébault, F. Gachon, I. Lemasson, C. Devaux, J. M. Mesnard, *J. Biol. Chem.* **275**, 4848–4857 (2000).
19. A. B. Byrne *et al*., *Sci. Transl. Med.* **14**, eabm4869 (2022).
20. M. Karlsson *et al*., *Sci. Adv.* **7**, eabh2169 (2021).
21. R. Syeda *et al*., *eLife* **4**, e07369 (2015).
22. C. M. Chen, N. Kraut, M. Groudine, H. Weintraub, *Cell* **86**, 731–741 (1996).
23. M. Moroni, M. R. Servin-Vences, R. Fleischer, O. Sánchez-Carranza, G. R. Lewin, *Nat. Commun.* **9**, 1096 (2018).
24. J. Wu *et al*., *Cell Rep.* **21**, 2357–2366 (2017).
25. K. Nonomura *et al*., *Proc. Natl. Acad. Sci. U.S.A.* **115**, 12817–12822 (2018).
26. E. Fotiou *et al*., *Nat. Commun.* **6**, 8085 (2015).
27. E. O. Anderson, E. R. Schneider, J. D. Matson, E. O. Gracheva, S. N. Bagriantsev, *Cell Rep.* **23**, 701–708 (2018).
28. Y. Xie *et al*., *Sci. Rep.* **6**, 28249 (2016).
29. A. Main, W. Fuller, *FEBS J.* **289**, 861–882 (2022).
30. W. Zheng, E. O. Gracheva, S. N. Bagriantsev, *eLife* **8**, e44003 (2019).
31. X. Yang *et al*., *Nature* **604**, 377–383 (2022).
32. J. Wang *et al*., *Cell Rep.* **38**, 110342 (2022).
33. C. Verkest, S. G. Lechner, *Curr. Opin. Physiol.* **31**, 100625 (2023).
34. L. Snider *et al*., *Mol. Cell. Biol.* **21**, 1866–1873 (2001).
35. J. Kazenwadel *et al*., *J. Clin. Invest.* **125**, 2979–2994 (2015).

ACKNOWLEDGMENTS

We thank B. Martinac, E. Perozo, J. Xu, and the Patapoutian Lab for useful scientific input and Y. Zhang and Y. Yuan for mass spec support. We thank the Cryo-EM Center at the Interdisciplinary Research Center on Biology and Chemistry of the Shanghai Institute of Organic Chemistry for help with data collection. **Funding:** This work was supported by Australian Research Council (ARC) Future Fellowship FT220100159 (C.D.C.); STI2030-Major Projects 2022ZD0207400, Shanghai Municipal of Science and Technology Project 20JC1419500, and Shanghai Municipal Science and Technology Major Project 2019SHZDZX02 (Y.Z.); National Health and Medical Research Council Ideas Grant 2021260 and the Lymphatic Malformation Institute (N.L.H.); ARC DP200100860 (B.C.); and Medical Research Future Fund grant GHFM76777 (H.S.S.). Research was undertaken with the assistance of resources and services from the National Computational Infrastructure, supported by the Australian Government. **Author contributions:** Z.Z., M.Y., and D.C. generated cell lines and performed biochemical and imaging experiments. Z.Z., N.B., and C.D.C. performed electrophysiology. G.A.S., D.L.S., H.S.S., V.J., R.P.H., and N.L.H. generated animal models and isolated cells. Z.Z. and J.V.L. generated reagents. X.M. and Y.Z. performed cryo-EM structural studies. B.C. and Y.L. performed molecular dynamics simulations. C.D.C. and Y.Z. conceived of and supervised the project. All authors wrote and approved the manuscript. **Competing interests:** C.D.C. and Z.Z. note an Australian provisional patent application #2023902096 entitled "Piezo channel regulators." **Data availability:** The composite map of the PIEZO1-MDFIC complex has been deposited in the Electron Microscopy Data Bank under the accession code EMD-35577. The composite map may contain artificial features near the boundaries of the masks. The consensus map, masked refined cap map, masked refined TMD map, and the map of PIEZO1-MDFIC (C240) have been deposited under the accession codes EMD-36241, EMD-36242, EMD-36243, and EMD-36244. The atomic coordinates have been deposited in the Protein Data Bank under the accession code 8IMZ. All data are available in the main text or the supplementary materials.

SUPPLEMENTARY MATERIALS

science.org/doi/10.1126/science.adh8190
Materials and Methods
Supplementary Text
Figs. S1 to S16
Tables S1 to S3
References (*36*–*47*)

Submitted 16 March 2023; accepted 19 July 2023
10.1126/science.adh8190